# High-purity thermoacoustic isotope enrichment

G. W. Swift,[a] D. A. Geller, and S. N. Backhaus
*Condensed Matter and Thermal Physics Group, Los Alamos National Laboratory, Los Alamos, New Mexico 87545*

(Received 24 March 2014; accepted 13 June 2014)

In a tube many wavelengths long, thermoacoustic separation of a gas mixture can produce very high purities. A flexible wall allows a spatially continuous supply of acoustic power into such a long tube. Coiling the tube and immersing it in a fluid lets a single-wavelength, circulating, traveling pressure wave in the fluid drive all the wavelengths in the tube wall and gas. Preliminary measurements confirm many aspects of the concept with neon ($^{20}$Ne and $^{22}$Ne) and highlight some challenges of practical implementation. © *2014 Acoustical Society of America*.
[http://dx.doi.org/10.1121/1.4887437]

PACS number(s): 43.35.Ud, 43.20.Mv, 43.35.Ty [RR] Pages: 638–648

## I. INTRODUCTION

When a sound wave travels through a gas mixture in a tube, oscillating radial thermal diffusion and oscillating axial motion combine to cause time-averaged flow of one component of the mixture in one axial direction while the other component flows in the opposite direction.[1–3] In experiments in a 1-m-long tube, a helium–argon mixture was separated to produce 40% end-to-end mole-fraction differences,[3] and a mixture of 91% $^{20}$Ne and 9% $^{22}$Ne (the natural abundances) was separated to produce 1% end-to-end mole-fraction differences in a 2-m-long tube.[4]

The steady-state gradient in the mole fraction $n$ of one component can be no larger than about[4]

$$\frac{dn}{dx} \sim (\gamma - 1)\,\frac{2\pi}{\lambda} k_T \sim (\gamma - 1)\,\frac{2\pi}{\lambda}\alpha_T n(1-n) \tag{1}$$

in a traveling wave, where $\lambda$ is the wavelength and $k_T = \alpha_T n(1-n)$ is the thermal diffusion ratio. The thermal diffusion constant $\alpha_T$ is

$$\alpha_{T\,\text{elastic spheres}} = \frac{105}{118}\frac{m_H - m_L}{m_H + m_L} \tag{2}$$

for a binary mixture of elastic-sphere atoms with heavy and light masses $m_H$ and $m_L$, to lowest order in the mass difference, and $\alpha_T$ in a mixture of real atoms with a small mass difference is typically about half of this value.[5]

As $n \to 0$, Eq. (1) is easily integrated to yield

$$n \sim e^{2\pi(\gamma-1)\,\alpha_T x/\lambda}. \tag{3}$$

Similarly, as $n \to 1$,

$$1 - n \sim e^{-2\pi(\gamma-1)\,\alpha_T x/\lambda}. \tag{4}$$

Thus, as the purity of a desired component becomes high, each tenfold improvement in purity (e.g., from 99.9% to 99.99%) requires a tube length

$$\Delta x_{10} \sim \frac{\ln 10}{2\pi(\gamma-1)\,\alpha_T}\lambda. \tag{5}$$

At best, $\Delta x_{10}$ is several wavelengths for a mixture such as He–Ar that has large $\gamma$ and large $\alpha_T$. For a more challenging mixture, such as an isotopic mixture of polyatomic molecules in which $\gamma$ is smaller and $\alpha_T$ is much smaller than in He–Ar, $\Delta x_{10}$ can be $100\lambda$ or more. Maintenance of a traveling wave in such a long tube is challenging because the separation process relies on the viscous and thermal boundary layers at the tube wall, which dissipate acoustic power. For a typical tube radius on the order of $5\delta$, where $\delta$ is either the viscous or thermal penetration depth, the amplitude of a traveling wave would be attenuated by about a factor of 3 every wavelength if acoustic power was not replenished along the way. The reliability and low cost of a thermoacoustic mixture separator might be seriously compromised if hundreds of separate sound sources had to be connected periodically to the tube to make up for this attenuation. (Six such sound sources were used in the one-wavelength-long tube of Ref. 4.)

We undertook the work described here to investigate the concept for high-purity thermoacoustic isotope enrichment illustrated in Fig. 1. We used natural-abundance neon in an enrichment tube 53 wavelengths long, coiled so each turn of the coil was one wavelength. The coil was immersed in water in a rigid torus-shaped vessel, and four speaker-driven bellows created a circulating pressure wave in the water that traveled around the torus. The tube's cross section was slightly oval, so its local cross-sectional area responded to the water pressure, slowing the water-wave propagation speed so it matched the neon's sound speed, while peristaltically driving the traveling wave in the neon within. Both the circulating water wave and the peristaltically driven neon wave resemble the "acoustitron" wave described in Ref. 6, where a more general theory of continuously driven toroidal wave propagation is developed and compared with an experiment using 32 transducers equally spaced around a closed loop of air-filled Tygon tubing.

Experiments and derivations described in the following text provide understanding of the coupled water and neon waves. Initial enrichment of the neon isotopes occurred as expected, but the poor reliability of this particular apparatus

[a]Author to whom correspondence should be addressed. Electronic mail: swift@lanl.gov

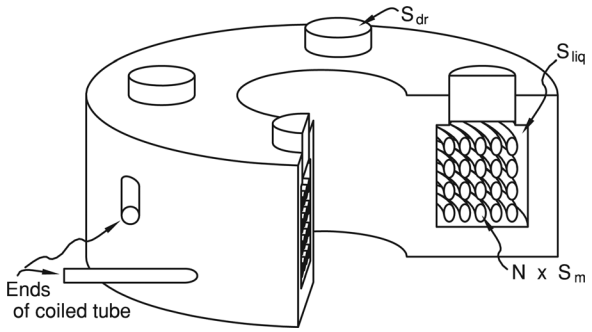


FIG. 1. $N$ circular coils of an oval tube, whose time-averaged cross-sectional area is $S_m$, are coiled in a toroidal, rigid-walled, water-filled vessel. In this illustration, $N = 20$, and the cutaway view exposes a water area $S_{liq}$, a total gas area $NS_m$, and a negligible tube-wall cross-sectional area. A few transducers driving the water (four transducers for this figure) create coupled traveling waves: A traveling wave one wavelength long in the water and a traveling wave $N$ wavelengths long in the coiled tube and the gas within it.

prevented observation of the very high purity of which this technique is capable.

## II. APPARATUS

We bought type-304, round, seamless stainless-steel tubing with outside diameter 3.4 mm and wall thickness 0.05 mm.[7] It was delivered in random lengths ranging from 1 to 3 m. After preliminary leak checks, we coiled each of these lengths to about 18 cm radius, simultaneously deforming the tubing cross section from circular to oval, with a custom-made, plastic tool resembling a tubing bender. We used short copper coupling tubes (and four brass fittings, described in the following text) and lead-free soft solder to join the lengths together into a long coil. Two hundred rubber o-rings slipped onto the tubing prevented turns of the coil from touching one another. Individual turns of the coiled tubing were tied, and later glued, to a few dozen short fiberglass posts to keep the coil manageable. The coil wound upward helically for about nine turns at one radius, then back downward about nine turns at a different radius, then upward and downward twice more for a total of about 53 turns. Inter-turn gaps were about half a tube diameter in the up/down direction and about one tube diameter in the radial direction.

Dozens of leaks developed in the tubing during the course of our work. About a third of the leaks were at the solder joints, a third where the tubing touched the fiberglass posts, and a third at locations that seemed unremarkable. One 4-mm-long, axial crack developed where the o-rings failed to prevent two turns of the coil from touching each other. Localizing and repairing these leaks was challenging because most surfaces of the tubing were hidden inside the coil, so the tubing accumulated many dents and kinks as our work proceeded. A few of the kinks were deep enough to block most of the cross section of the tubing. Furthermore, one accidental moment of very high pressure in the surrounding water flattened about 25% of the tubing. Subsequently raising the pressure inside the tubing to 6.5 bar (gauge) brought the flattened portions back to oval cross section (and, incidentally, improved the aspect-ratio uniformity of the unflattened portions). After all of these misfortunes, the coil was 53.25 turns long with a radius of curvature ranging from 16 cm near one end to 19 cm near the other end, giving a total length (including fittings) of 60 m. Each turn of the coil had at least one patch, joint, dent, or kink. The outside major and minor axes of the tube's oval cross section were $3.95 \pm 0.1$ and $2.73 \pm 0.1$ mm, respectively, and the wall thickness was $50 \pm 5$ $\mu$m.

Four piezoresistive pressure transducers[8] were mounted in brass fittings at the ends of the coil and at 17.75 turns from the ends, allowing measurements of the neon mean pressure and acoustic pressures. Copper tubes with 0.9 mm inner diameter (i.d.) led from these fittings through 10-$\mu$m-i.d. flow impedances and a valve network to a residual gas analyzer[9] to measure the neon-isotope mole fractions at those four locations, as described in Ref. 3.

The coil was immersed in a torus-shaped acoustic water cavity in an anodized-aluminum vessel, which was made of an inner cylinder, an outer annulus, and top and bottom plates, all bolted together and sealed with rubber o-rings. The water cavity's inner radius was 14.9 cm, its outer radius was 20.1 cm, and its height was 9.8 cm. The fiberglass posts supporting the coil were pressed into holes in one of the flat surfaces of this cavity. Four more piezoresistive pressure transducers,[8] equally spaced azimuthally, sensed the water acoustic pressure on that same flat surface, and the opposite flat surface had four 2-cm-diameter holes leading to four nickel bellows[10] soldered shut with brass seals that were epoxied to loudspeakers[11] to drive the sound wave in the water. To create a circulating water-pressure wave by driving the speakers with phases of 0°, 90°, 180°, and 270°, we used two function generators phase-locked with 90° between them, feeding their sinusoidal signals into the two channels of a stereo amplifier. Each channel of the amplifier fed two of the speakers with polarities reversed. The direction of propagation of the water-pressure wave could be easily reversed by changing the sign of the 90° phase difference between the function generators.

Two speakers overheated and burned out during the course of the measurements. To prevent further failures, we glued a few wraps of copper tubing to the magnet of each speaker and circulated 20 °C water through them thereafter.

Removing air from the water in the toroidal acoustic cavity was essential to prevent the compressibility of air bubbles from affecting the water-wave propagation and to reduce the likelihood of cavitation-induced damage to the tubing. Evacuating the acoustic cavity and letting it fill with degassed water was unsuccessful: This process always caused audible water hammer and usually caused immediate leaks in the neon tubing's solder joints no matter how slowly we tried to admit the water. A more complicated process based on the temperature dependence of the solubility of air in water worked well: The apparatus was tilted about 5°, and water (tap water with a few drops of dish detergent) was added through a fitting on the downhill side while air escaped from another fitting at the top of the uphill side. Next, components were attached to form a recirculating loop: A pot full of water, with a loose-fitting lid, was maintained at 75 °C by electric heat. The free surface of the water in this pot was about 50 cm above the top of the acoustic cavity. The water flowed from the bottom of this pot to a heat exchanger maintained at 20 °C and then into the

downhill side of the acoustic cavity. Coming out at the uphill side, the water flowed through a circulating pump, a flow meter, a flow impedance adjusted so 2 $cm^3$/s of water circulated, and finally back into the pot. The 75 °C pot ensured that the water entering the acoustic cavity could have only 7 $cm^3$ of dissolved air per liter of water, leaving it capable of dissolving and removing an additional 12 $cm^3$/l in the 20 °C cavity. The slowly flowing water may not have reached all corners of the acoustic cavity, but maintaining this circulation for a week or more led to reproducible, understandable acoustics in the cavity as remote bubbles slowly dissolved. We continued this circulation throughout the experiments, so any neon leaking into the water would also be removed.

Atmospheric pressure in Los Alamos is about 80 kPa. The mean pressure in the water was about 0.5 m of water head higher, i.e., about 85 kPa. All experiments were performed with the neon mean pressure at about 90 kPa.

## III. ACOUSTICS

The high-purity isotope-enrichment concept shown in Fig. 1 relies on coordination among the flexibility of the tubing wall, the acoustics in the toroidal, water-filled cavity, and the acoustics in the isotopic mixture to be enriched. In this section, we derive expressions for the relevant acoustics and present low-amplitude measurements confirming these expressions. The first subsection describes the acoustics in the gas and the flexing tube wall, and the second subsection describes the acoustics in the water-filled cavity.

### A. Oval peristaltic tube acoustics

Consider wave propagation in the $x$ direction in a gas within a tube, as shown in Fig. 2(a), with a cross-sectional area $S$ that varies with $x$ and time $t$ according to

$$S(x,t) = S_m + \mathrm{Re}\left[S_1(x)e^{i\omega t}\right], \tag{6}$$

using the complex notation[12] that is often used for the $x$ and $t$ dependences of other thermoacoustic variables such as pressure $p$, laterally averaged axial velocity $\langle u\rangle$, laterally averaged density $\langle\rho\rangle$, and laterally averaged temperature $\langle T\rangle$. Examination of derivations[12] of the equations for oscillating, laterally averaged momentum density $\rho_m\langle u_1\rangle$ and oscillating temperature $\langle T_1\rangle$ show that to first order they are not affected by nonzero $S_1$, so these equations remain

$$\frac{dp_1}{dx} = -\frac{i\omega\rho_m}{1-f_\nu}\langle u_1\rangle, \tag{7}$$

$$\langle T_1\rangle = \frac{1}{\rho_m c_p}(1-f_\kappa)p_1, \tag{8}$$

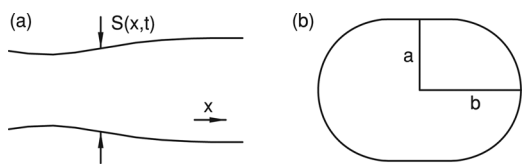


FIG. 2. (a) A tube extending in the $x$ direction with a variable area $S(x,t)$. (b) A tube with racetrack-shaped oval cross section with semi-minor axis $a$ and semi-major axis $b$.

where $f_\nu$ and $f_\kappa$ are the thermoviscous functions that account for the spatial averaging over area $S_m$ and $c_p$ is the isobaric specific heat. In Eq. (8) and throughout this paper, we take $dT_m/dx = 0$, and, to keep the mathematics simple, we neglect the fact[1–3] that gas mixtures involve $f_{\kappa D}$ and $f_{D\kappa}$ instead of just $f_\kappa$, the differences being small for small $\alpha_T$. The first-order continuity equation[13] depends significantly on $S_1$,

$$0 = i\omega\frac{\langle\rho_1\rangle}{\rho_m} + \frac{d\langle u_1\rangle}{dx} + i\omega\frac{S_1}{S_m}, \tag{9}$$

showing how oscillating area $S_1$ can drive a combination of oscillating density and $d\langle u_1\rangle/dx$. Using the first-order equation of state to express $\langle\rho_1\rangle$ in Eq. (9) in terms of $p_1$, $\langle T_1\rangle$, and the adiabatic sound speed $c_{\mathrm{gas}}$, and using Eq. (8) for $\langle T_1\rangle$, yield

$$\frac{d\langle u_1\rangle}{dx} = -i\omega\frac{S_1}{S_m} - \frac{i\omega}{\rho_m c_{\mathrm{gas}}^2}\left[1+(\gamma-1)f_\kappa\right]p_1 \tag{10}$$

for the thermoacoustic continuity equation with a time-dependent cross-sectional area $S$. The corresponding Helmholtz equation is formed by substituting Eq. (10) into the $x$ derivative of Eq. (7) to obtain

$$(1-f_\nu)\frac{c_{\mathrm{gas}}^2}{\omega^2}\frac{d^2p_1}{dx^2} + \left[1+(\gamma-1)f_\kappa\right]p_1 = -\rho_m c_{\mathrm{gas}}^2\frac{S_1}{S_m}. \tag{11}$$

To model a traveling wave with $x$-independent gas properties in a tube of infinite length, one can use

$$p_1 = p_{1A}e^{\pm ikx}, \tag{12}$$

$$S_1 = S_{1A}e^{\pm ikx}, \tag{13}$$

where $|p_{1A}|$ and $|S_{1A}|$ are the $x$-independent amplitudes of the pressure and area waves, respectively, the phases of $p_{1A}$ and $S_{1A}$ simply give the time phases of those variables at $x = 0$, $k$ is the (real) wavevector of the wave, and the negative signs correspond to a wave traveling in the positive-$x$ direction. Substituting these into the Helmholtz equation and using $\rho_m c_{\mathrm{gas}}^2 = \gamma p_m$ for an ideal gas yield

$$\frac{p_{1A}}{\gamma p_m} = \frac{S_{1A}/S_m}{(1-f_\nu)\left[k^2-(k_0-i\alpha)^2\right]c_{\mathrm{gas}}^2/\omega^2}, \tag{14}$$

where

$$k_0 = \frac{\omega}{c_{\mathrm{gas}}}\mathrm{Re}\left[\sqrt{\frac{1+(\gamma-1)f_\kappa}{1-f_\nu}}\right], \tag{15}$$

$$\alpha = -\frac{\omega}{c_{\mathrm{gas}}}\mathrm{Im}\left[\sqrt{\frac{1+(\gamma-1)f_\kappa}{1-f_\nu}}\right]. \tag{16}$$

At this point in the analysis, $\omega$ and $k$ remain independent of each other because the mechanism by which the tube is driven has not yet been specified.

In the boundary-layer approximation in a tube with hydraulic radius $r_h$, the thermoviscous functions are $f_j$

$\simeq (1-i)\delta_j/2r_h$, so $k_0 \simeq \left[1+(\gamma-1+\sqrt{\sigma})\,\delta_\kappa/4r_h\right]\omega/c_{\rm gas}$ and $\alpha \simeq \left[(\gamma-1+\sqrt{\sigma})\,\delta_\kappa/4r_h\right]\omega/c_{\rm gas}$, where $\sigma$ is the Prandtl number. Equation (14) then shows that high pressure amplitudes can be reached with only modest area changes when

$$\omega \sim k c_{\rm gas}. \tag{17}$$

In other words, at any given frequency $\omega$, it is best to drive the tube wall with a wavelength $2\pi/k$ that matches the gas wavelength inside. For the typical enrichment-tube size on the order of $2r_h \simeq 5\delta_\kappa$, and taking $\gamma = 5/3$ and $\sigma \simeq 2/3$ for a monatomic gas, the best condition is $\omega \simeq 0.9kc_{\rm gas}$, for which Eq. (14) yields

$$\frac{p_{1A,\rm best}}{\gamma p_m} \sim -3i\frac{S_{1A}}{S_m}, \tag{18}$$

so a wave with $|p_{1A}|/p_m \sim 0.05$ can be maintained in a monatomic gas by driving the tube with only $|S_{1A}|/S_m \sim 0.01$. Coming close to this best condition may be important to minimize flexing fatigue in the tube wall during long-term operation.

The time-dependent cross-sectional area $S(x,t)$ expressed by Eq. (6) can be achieved in a flexible, thin-walled tube with an oval cross section, as shown in Fig. 2(b), if it is subject to a time-dependent external pressure

$$P(x,t) = p_m + {\rm Re}\left[P_{1A}e^{\pm ikx}e^{i\omega t}\right]. \tag{19}$$

Let $a$ and $b$ be the semi-minor and semi-major axes, respectively, of the tube with racetrack-shaped oval cross section shown in Fig. 2(b), and define

$$\epsilon = b/a - 1. \tag{20}$$

Appendix A shows the derivation of the proportionality constant between area changes and pressure changes for such a tube. (A racetrack-shaped tube instead of an elliptical tube is analyzed because the mathematics seems easier for the racetrack and because the cross section of our tube turned out to more closely resemble a racetrack than an ellipse.) Using $p - P$ wherever $p$ appears in Appendix A, the result is

$$\frac{S_{1A}}{S_m} = \frac{p_{1A} - P_{1A}}{\beta E}, \tag{21}$$

where $E$ is the elastic modulus of the tube-wall material and where the geometrical part of the proportionality constant is given by

$$\beta \cong \frac{0.44h^3}{\epsilon^2 a^3}\frac{1+1.91\epsilon+0.81\epsilon^2}{1+3.36\epsilon+2.85\epsilon^2+0.90\epsilon^3+0.30\epsilon^4}, \tag{22}$$

with $h$ the wall thickness. (For the circumstances of the experiments described in this paper, inertial corrections to this analysis are negligible.)

Combining Eqs. (14) and (21) shows that

$$\frac{P_{1A}}{p_{1A}} = 1-(1-f_\nu)\left[k^2-(k_0-i\alpha)^2\right]\frac{c_{\rm gas}^2}{\omega^2}\frac{\beta E}{\gamma p_m}. \tag{23}$$

For our tube, $\beta E \gg \gamma p_m$, so the first "1" on the right-hand side is negligible. In the boundary-layer approximation, and near the best condition $k \sim \omega/c_{\rm gas}$, Eq. (23) becomes

$$\left|\frac{P_{1A}}{p_{1A}}\right|_{\rm best} \sim (\gamma-1+\sqrt{\sigma})\,\frac{\delta_\kappa}{2r_h}\frac{\beta E}{\gamma p_m}. \tag{24}$$

Substituting the tube dimensions given in Sec. II into Eq. (22) and using $E = 193$ GPa for stainless steel yields $\beta E = 14.2$ MPa for our tube. To measure the actual response of the tubing cross-sectional area to pressure, we vented the water cavity to atmospheric air through a pipette and observed the water level in the pipette as the neon pressure was varied. The pipette was horizontal, with surface tension maintaining a well-defined meniscus, to keep the water pressure constant so the driver bellows' response to water pressure was irrelevant. The measurements showed that the enrichment tube expanded with pressure at a rate of 0.00446 cm$^3$/torr, corresponding to $\beta E = 15.4$ MPa. The 9% difference between the calculated and measured values of $\beta$ may be due to some combination of the damage suffered by the tube during handling, the noncompliance of the many soldered fittings and patches, and the fact that the tube's cross section was not exactly racetrack-shaped. In further analysis in this section, the experimental value of $\beta E$ is used.

Figure 3 shows a comparison of the magnitude and phase of the inverse of Eq. (23) to corresponding measurements in our apparatus as functions of frequency, with the speakers driven as described in Sec. II. The measurements were made quickly, with the speakers' drive voltage fixed at only 8% of what would later be used for isotope enrichment, so the neon isotopes could not separate significantly during the course of these measurements. Shown in Fig. 3 are measurements at the two neon pressure transducers that were 17.75 turns from

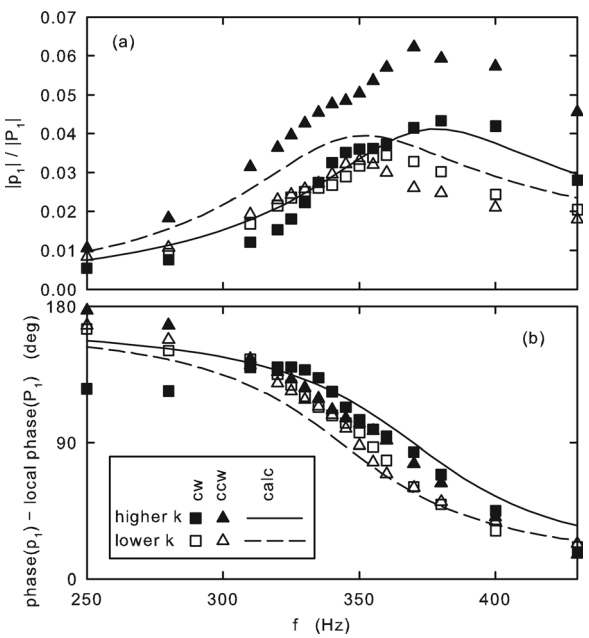


FIG. 3. (a) Relative magnitude and (b) relative phase of neon pressure $p_1$ and water pressure $P_1$ at the two locations 17.75 turns from the nearest end of the enrichment tube as functions of frequency $f$. Points represent measurements; curves represent Eq. (23). The measurements include two directions of wave propagation, which we call clockwise and counterclockwise.

the ends of the coil. For each sensor, two directions of wave propagation are possible, yielding a total of four sets of data. The radius of curvature of the coil near one transducer (whose measurements are indicated by the solid symbols) made the wavevector in its vicinity $k = 5.8\ \mathrm{m}^{-1}$, and that near the other transducer (open symbols) was $5.4\,\mathrm{m}^{-1}$; these values were used in Eq. (23) to generate the solid and dashed curves, respectively. We used the boundary-layer expressions for $f_\nu$ and $f_k$ in Eqs. (15), (16), and (23).

Qualitatively, the experimental data in Fig. 3 show a resonance when $c/f$ in the neon matches the driving wavelength, i.e., the length of one turn of the coil, with a quality factor on the order of $r_h/\delta$. The quality factors and the resonance frequencies are in quantitative agreement[14] with the calculations based on Eq. (23). In particular, the higher-$k$ location has a higher resonance frequency. The fact that the clockwise and counterclockwise waves have different amplitudes, especially at the higher-$k$ location, may be due to the damage suffered by the tubing during handling before these measurements were obtained.

Equation (23) is valid for a tube of infinite length. For a tube of finite length $L$ sealed at both ends so $dp_1/dx = 0$ at $x = 0$ and $x = L$, the general solution to Eq. (11) is

$$p_1(x) = p_{1A}e^{\pm ikx} - Ae^{-(ik_0+\alpha)x} - Be^{(ik_0+\alpha)(x-L)}, \tag{25}$$

where $S_1$ and $p_{1A}$ are still given by Eqs. (13) and (14), respectively, and

$$A = \mp\, p_{1A}\frac{k}{k_0 - i\alpha}\frac{1 - e^{-(ik_0 \mp ik+\alpha)L}}{1 - e^{-2(ik_0+\alpha)L}}, \tag{26}$$

$$B = \pm\, p_{1A}\frac{k}{k_0 - i\alpha}\frac{e^{\pm ikL} - e^{-(ik_0+\alpha)L}}{1 - e^{-2(ik_0+\alpha)L}}. \tag{27}$$

When $\alpha L \gg 1$, the second term in Eq. (25) is non-negligible only near $x = 0$, and the third term is non-negligible only near $x = L$. Because $\alpha \sim 1/\lambda$, both of these terms are negligible more than a few wavelengths from the ends, so the use of Eq. (23) in Fig. 3 is justified. Figure 4 shows the corresponding experimental and calculated results at the ends of our tube, where the wavevectors were 5.3 and $6.1\,\mathrm{m}^{-1}$, with the calculations based on Eq. (25), neglecting the $x$ dependence of $p_1$ in Eq. (21) because $|p_1| \ll |P_1|$. For each direction of propagation of the wave in the tube, there is a high-amplitude end, toward which the wave travels and from which it reflects, and a low-amplitude end, away from which the wave travels. At the high-amplitude end, $|p_1|/|P_1|$ is double its value in Fig. 3, and the $k$ dependence of the results due to the varying radius of curvature of the coil is even more apparent than in Fig. 3. We suspect that the extra-high amplitudes of the counterclockwise, highest-$k$ measurements and of the low-amplitude-end measurements[14] are due to damage in the tube, giving short regions near the ends unusually high or low compliance.

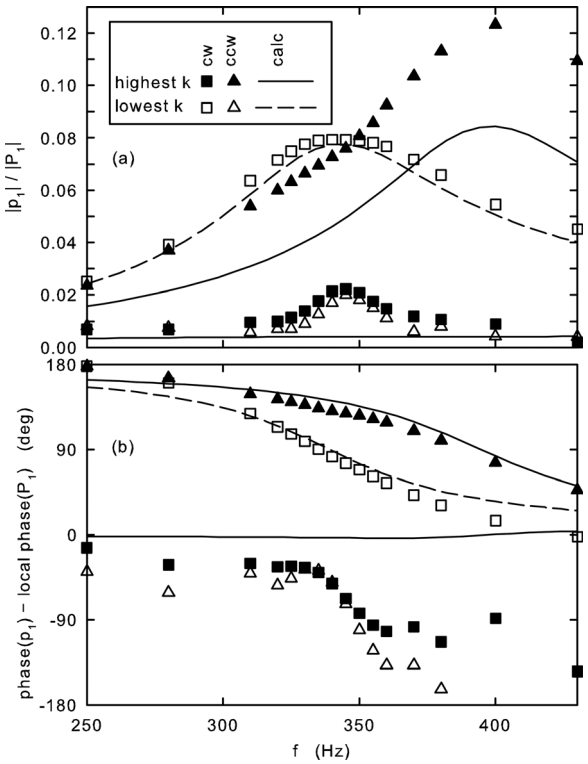


FIG. 4. (a) Relative magnitude and (b) relative phase of neon pressure $p_1$ and water pressure $P_1$ at the two ends of the enrichment tube, as functions of frequency $f$. Points represent measurements; curves represent Eqs. (25), (21), and (14). The measurements include two directions of wave propagation, which we call clockwise and counterclockwise. [In both (a) and (b), the solid and dashed curves for the low-amplitude end of the tube are near zero and are indistinguishable from each other.]

## B. Coupled water–tube acoustics

With the enrichment tube coiled in the water cavity, the wavevector $k$ first used in Eq. (12) must equal $2\pi$ (or $4\pi$, $6\pi$,…) divided by the circumference $\lambda_{\mathrm{torus}}$ of the torus, and then the high gas-pressure amplitude given in Eq. (18) can be achieved by choosing the frequency to make $\omega \sim kc_{\mathrm{gas}}$. In this section, we analyze this coupled system from the water's perspective to understand the relationships between the wave in the water and those in the tubing wall and in the gas. We continue to assume that a single $k$ is a good-enough approximation even though our apparatus actually used a range of $k$ because of the range of coil radii.

The wave in the water in Fig. 1 obeys an equation adapted from Eq. (11),

$$\frac{c_{\mathrm{liq}}^2}{\omega^2}\frac{d^2P_1}{dx^2} + P_1 = \rho_{\mathrm{liq}}c_{\mathrm{liq}}^2\frac{NS_1}{S_{\mathrm{liq},m}} - \rho_{\mathrm{liq}}c_{\mathrm{liq}}^2\frac{S_{\mathrm{liq},1}}{S_{\mathrm{liq},m}}. \tag{28}$$

The coordinate $x$ in the water runs parallel to the coordinate $x$ in the oval tube, $P$ is the pressure in the water, $S_{\mathrm{liq}}$ is the effective cross-sectional area of the water cavity, and $\rho_{\mathrm{liq}}$ and $c_{\mathrm{liq}}$ are the density and sound speed in the water. We have neglected the boundary dissipation factors involving $f_\nu$ and $f_\kappa$ that appeared in Eq. (11) because we expect that the dominant sink of acoustic power here is the coupling of acoustic power from the water into the oval tube. The signs of the two terms on the right-hand side differ because an increase in $S_1$ decreases the area available to the water while an increase in $S_{\mathrm{liq},1}$ increases this available area. For a finite number $M$ of drivers exciting the water wave (Fig. 1 shows

$M = 4$), equally spaced along the circumference of the torus, each of which has area $S_{dr}$ and moves with complex displacement amplitude $\xi_{dr,1}$ (positive downward in Fig. 1) with equally spaced time phasing, we use the approximation that

$$S_{\mathrm{liq},1} \simeq -\frac{MS_{dr}}{\lambda_{\mathrm{torus}}}\xi_{dr,1}. \tag{29}$$

With all of the first-order variables proportional to $e^{\pm ikx}$, using Eq. (21) to express $S_{1A}$ in terms of $p_{1A}$ and $P_{1A}$, and using Eq. (29) for $S_{\mathrm{liq},1}$, Eq. (28) becomes

$$\left(\frac{NS_m\omega/k}{\beta E} - \frac{S_{\mathrm{liq},m}}{\rho_{\mathrm{liq}}\omega/k} + \frac{S_{\mathrm{liq},m}\omega/k}{\rho_{\mathrm{liq}}c_{\mathrm{liq}}^2}\right)P_{1A} - \frac{NS_m\omega/k}{\beta E}p_{1A} = \frac{MS_{dr}\omega/k}{\lambda_{\mathrm{torus}}}\xi_{dr,1A}. \tag{30}$$

The three terms on the left-hand side in the $P_{1A}$ term represent lossless water acoustics in this system. The inertance per unit length of the water is $\rho_{\mathrm{liq}}/S_{\mathrm{liq},m}$, so the second term is the inverse of the inertial impedance of the water in length $\lambda/2\pi$. Similarly, the third term is the inverse of the compliant impedance in length $\lambda/2\pi$ caused by the compressibility of the water. The first term represents the compressibility of the enrichment tube, neglecting any properties of the gas inside it. If $\omega$ is chosen near the best value given in Eq. (17), then the ratio of the third to the second term is $c_{\mathrm{gas}}^2/c_{\mathrm{liq}}^2 \ll 1$, so the lossless water acoustics is readily interpreted as a propagation of the inertia of the water against the compressibility of the oval enrichment tube with the compressibility of the water itself being negligible. Careful choice of $S_{\mathrm{liq},m}$ can make the coefficient of $P_{1A}$ in Eq. (30) zero, so resonance in the water/tube-wall system can make the $P_{1A}$ term disappear, with $\xi_{dr,1A}$ seeming to couple directly to $p_{1A}$ in the gas in the enrichment tube.

For a fixed value of $S_{\mathrm{liq},m}$, Eq. (30) shows that the water pressure $P_1$ should be a resonant function of frequency, as the drivers see mostly tube compliance at high frequency, mostly water inertia at low frequency, and mostly the effect of the $p_{1A}$ term at the resonance frequency. Figure 5 shows the experimental results for $P_1$ as a function of frequency, for constant driver voltage (the same as for Figs. 3 and 4, i.e., 8% of the voltage used for the subsequent isotope-enrichment measurements). Setting the $P_{1A}$ term in Eq. (30) equal to zero and solving for $\omega$, using the known geometry of the apparatus and the value for $\beta E$ obtained with the pipette measurement, yields a predicted resonance frequency of 341 Hz, in excellent agreement with the measured values shown in Fig. 5: 350 Hz for the 0°–180° sensors and 345 Hz for the 90°–270° sensors. We judged this observed water–tube resonance frequency to be close enough to the range of neon resonances shown in Figs. 3 and 4 (340 Hz at one end of the tube, 400 Hz at the other end) that we did not change $S_{\mathrm{liq},m}$, and we adopted 350 Hz for the later enrichment experiments.

The quality factor of the resonances shown in Fig. 5(a) is about 15. This should equal $\omega$ times the ratio of the energy stored in the resonance to the rate of energy

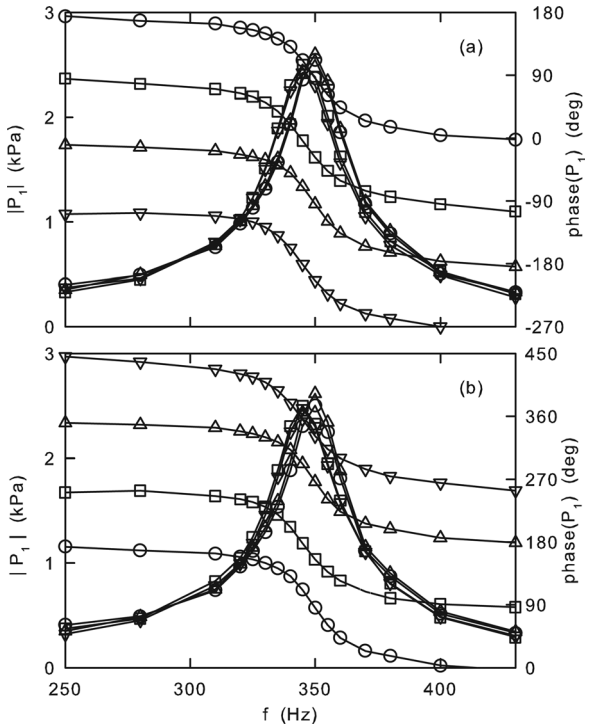


FIG. 5. Magnitudes (peaks; left axes) and phases (monotonically decreasing curves; right axes) of water acoustic pressure $P_1$ for (a) clockwise and (b) counterclockwise propagation of the waves, as functions of frequency $f$. Circles, pressure sensor at speaker whose voltage phase is defined to be zero for this figure; squares, sensor 90° clockwise from that sensor; erect triangles, 180° clockwise; inverted triangles, 270° clockwise. The lines are only guides to the eye.

dissipation. In this toroidal traveling resonance, every location has stored energy independent of time, the stored energy at every location shifting twice each cycle between kinetic energy in the water and compressive energy in the tube-wall stress. Mechanisms for power dissipation include the boundary-layer losses in the neon in the enrichment tube and the viscous boundary-layer losses in the water on the surface areas of the water cavity and the enrichment tube. Straightforward calculations of these quantities yield a quality factor of 23, with the dissipation in the neon being 15 times higher than that in the water. Additional dissipation could be coming from acoustic power radiated into the room, into the tubes carrying the recirculating water into and out of the water cavity, and into any tight-entranced pockets in the water cavity that might have retained trapped air, such as under the fiberglass posts.

Near Eq. (18) in the preceding text, we discussed how to minimize $|S_{1A}|/|p_{1A}|$, keeping flexure stress in the enrichment tube to a minimum. Under that condition, substituting Eqs. (21) and (18) into Eq. (30) (and neglecting the $1/c_{\mathrm{liq}}^2$ term to simplify the math) shows how to minimize $|\xi_{1A}|/|S_{1A}|$, thereby also keeping the displacement of the drivers to a minimum,

$$\left[\frac{3i\gamma p_m}{\rho_{\mathrm{liq}}\omega^2/k^2} - \left(\frac{NS_m}{S_{\mathrm{liq},m}} - \frac{\beta E}{\rho_{\mathrm{liq}}\omega^2/k^2}\right)\right]\frac{S_{1A}}{S_m} = \frac{MS_{dr}\xi_{1A}}{S_{\mathrm{liq},m}\lambda_{\mathrm{tor}}}. \tag{31}$$

For our tube, $\beta E \gg \gamma p_m$, so the best $S_{\mathrm{liq},m}$ is essentially that found by setting the term in parentheses equal to zero, yielding

$$S_{\mathrm{liq},m,\mathrm{best}} \simeq N S_m \frac{\rho_{\mathrm{liq}} \omega^2 / k^2}{\beta E}. \tag{32}$$

This is, again, the resonance condition obtained by setting the coefficient of the $P_{1A}$ term in Eq. (30) equal to zero (still neglecting $1/c_{\mathrm{liq}}^2$).

## IV. ISOTOPE ENRICHMENT

With a traveling wave established in a long enrichment tube as described in Sec. III, a significant mole-fraction gradient should develop with time. In this section, we consider that development.

The mole flux of the heavy component is given by Eq. (A1) in Ref. 4,

$$\dot{N}_H(x,t) = \frac{\delta_\kappa}{4 r_h} \frac{\gamma - 1}{\gamma} \frac{\alpha_T n_H (1 - n_H) S_m}{R_{\mathrm{univ}} T} |p_1| |\langle u_1 \rangle| (F_{\mathrm{trav}} \cos\theta + F_{\mathrm{stand}} \sin\theta) + \frac{\rho_m S_m}{m_{\mathrm{avg}}} \left( \frac{\delta_\kappa}{4 r_h} \frac{|\langle u_1 \rangle|^2}{\omega} F_{\mathrm{grad}} - D_{12} \right) \frac{\partial n_H}{\partial x}, \tag{33}$$

where $m_{\mathrm{avg}}$ is the average molar mass, $\theta$ is the phase by which $p_1$ leads $\langle u_1 \rangle$, and $D_{12}$ is the mutual mass-diffusion coefficient. Boundary-layer expressions for the three $F_j$, all of which are negative, are given in Ref. 4. The $|p_1||\langle u_1 \rangle|$ term on the right-hand side expresses the tendency of the wave to create a separation mole flux and a nonzero mole-fraction gradient. The second term expresses the competing tendency of both $D_{12}$ and nonzero $\langle u_1 \rangle$ to limit or reduce such a mole-fraction gradient.

The time evolution of $n_H(x,t)$ is governed by one additional equation, which expresses conservation of heavy atoms, i.e., that $n_H$ can change in time at any location only if there is a local gradient in its flux,

$$\frac{\partial n_H}{\partial t} + \frac{m_{\mathrm{avg}}}{\rho_m S_m} \frac{\partial \dot{N}_H}{\partial x} = 0. \tag{34}$$

Equation (7) shows that $p_1$ and $\langle u_1 \rangle$ are not exactly in phase in a traveling wave in a tube because of viscous effects at the wall, so $F_{\mathrm{stand}}$ is involved in the "traveling" mixture-separation process in a small way. To accommodate this with minimal algebraic clutter, note that $p_1$ lags $\langle u_1 \rangle$ by $\delta_\nu / 2 r_h$ in the boundary-layer approximation, so define

$$F'_{\mathrm{trav}} = F_{\mathrm{trav}} - F_{\mathrm{stand}} \delta_\nu / 2 r_h. \tag{35}$$

Combining Eqs. (7), (12), (34), (35), and the $x$ derivative of Eq. (33) yields

$$\frac{\partial n_H}{\partial t} - (1 - 2 n_H) U \frac{\partial n_H}{\partial x} = D \frac{\partial^2 n_H}{\partial x^2}, \tag{36}$$

where

$$U = -\frac{\delta_\kappa}{4 r_h} \frac{c_{\mathrm{gas}} k}{\omega} (\gamma - 1) \alpha_T F'_{\mathrm{trav}} \frac{|p_{1A}|^2}{\gamma^2 p_m^2} c_{\mathrm{gas}}, \tag{37}$$

$$D = -\frac{\delta_\kappa}{4 r_h} \left( \frac{c_{\mathrm{gas}} k}{\omega} \right)^3 F_{\mathrm{grad}} \frac{|p_{1A}|^2}{\gamma^2 p_m^2} \frac{c_{\mathrm{gas}}}{k} + D_{12}. \tag{38}$$

The signs are chosen to make $U$ and $D$ positive, despite the $F_j$ being negative. The initial and boundary conditions relevant to our apparatus, filled with an originally uniform mixture and sealed at both ends, can be written

$$n_H(x,0) = n_{\mathrm{fill}}, \tag{39}$$

$$0 = \dot{N}_H \propto U n_H (1 - n_H) + D \frac{\partial n_H}{\partial x} \quad \text{at } x = 0 \text{ and } x = L. \tag{40}$$

Appendix B analyzes limits of Eq. (36) for which we have found analytical solutions satisfying conditions (39) and (40).

We can gain intuition about this thermoacoustic isotope-enrichment situation by recognizing that the low-$n_H$ limit of Eq. (36), in which the $2 n_H$ term can be neglected, is the convection-diffusion equation (also called the advection-diffusion equation). It is a one-dimensional diffusion equation with diffusivity $D$ superimposed on motion toward negative $x$ with velocity $U$. Thus this problem [including its initial and boundary conditions, Eqs. (39) and (40)] is analogous to a fixed mass of solute, initially uniformly distributed, trapped between semi-permeable membranes in a pipe, with a solvent moving at velocity $U$ carrying the solute in the negative-$x$ direction, while the trapped solute diffuses with diffusivity $D$. This suggests that a time $L/U$ should characterize the approach to steady state. For $D = 0$, all of the solute could have accumulated sharply at the downstream end of the tube after time $L/U$, but nonzero $D$ diffuses the solute back upstream. As $t \to \infty$, the balance between $U$ and $D$ creates an exponential mole-fraction profile, with tenfold change of mole fraction in each tube length of $(D/U)\ln 10$. [Cf. the characteristic length given by Eq. (5) with "best" condition $\omega = c_{\mathrm{gas}} k$.] For conditions of our measurements, i.e., at $|p_{1A}| = 0.7$ kPa, Eqs. (37) and (38) yield $U = 4$ $\mu$m/s and $D = 10^{-4}$ m$^2$/s, so $L/U$ is 6 months and $(D/U)\ln 10$ is the length of the tube. A higher, reasonable value of $|p_{1A}| = 4.5$ kPa would reduce this to 4 days and half of the length of the tube.

Other aspects of Eq. (36) can be interpreted using this analogy to superimposed convection and diffusion. Qualitatively, the $2 n_H$ term in Eq. (36) merely reduces the effective $U$ a little, in an $x$-dependent way, slowing the approach to steady state and increasing the length of tube

required for each tenfold enrichment. Near the ends of the tube, where $|p_1|$ depends on $x$ as described by Eq. (25), $U$ and $D$ also vary with $x$. Approaching the low-amplitude end, $(D/U)\ln 10$ grows because $D \to D_{12}$ while $U$ decreases exponentially, so the steady-state mole-fraction gradient is reduced there. (The time needed for that region to equilibrate with the nearby, full-amplitude part of the tube would be of order $\lambda^2/D_{12}$, not prohibitively long.) Approaching the high-amplitude end, the situation is more complicated. Equations (25) and (7) show $|p_1(x)|$ and $|\langle u_1(x)\rangle|$ oscillating out of phase, twice per wavelength, with increasing amplitude as the reflecting end is approached. The phase between $p_1$ and $\langle u_1\rangle$ also oscillates with increasing amplitude, reaching $\pm 90^\circ$ at the reflecting end, so $F_{\text{stand}}$ becomes involved strongly enough to affect $dn_H/dx$ noticeably, even changing its sign in the final quarter wavelength. Calculations based on Eq. (25) for our apparatus at $|p_{1A}| = 0.7$ kPa in mid-tube show that about one wavelength at each end of our tube is effectively useless for establishing the end-to-end mole-fraction difference.

We learned quickly that our tube often developed leaks, so we began with measurements at relatively low amplitude: $|p_{1A}| = 0.7$ kPa in mid-tube. At that amplitude, Fig. 6 shows measurements of the $^{22}$Ne mole fraction at four places in the tube, together with a numerical integration[15] of Eq. (36) with boundary conditions (39) and (40) (solid curves), and the low-$n_H$ calculations based on Eqs. (B12) and (B15) (dashed curves). The measurements at the ends of the tube are in reasonable agreement with the corresponding calculations. The differences between the filled and open symbols, representing data taken months apart with different levels of tubing damage, may be indicative of how strongly tubing damage can affect the enrichment process. At these short times, the mole fraction at the mid-tube locations should hardly have changed at all, but the data show non-negligible changes, especially at the $x = 2L/3$ location. We speculate that tubing damage caused local distortion in $p_1(x)$, which in turn caused local mole-fraction gradients to develop rapidly, and that these local gradients would not interfere with longer-term enrichment. The fact that the slopes of the measurements at these locations from about 4 to 8 days are small—comparable to the slopes of the corresponding calculations—lends some support to this speculation.

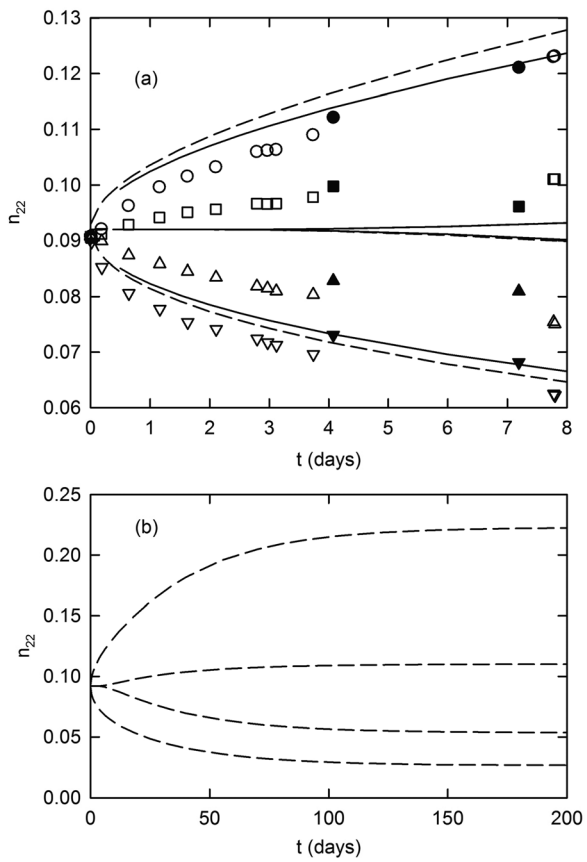


FIG. 6. Points show measured $^{22}$Ne mole fractions as functions of time for a clockwise wave with a mid-tube pressure amplitude of 0.7 kPa at four locations: Circles, $x = 0$; squares, $x = L/3$; triangles, $x = 2L/3$; inverted triangles, $x = L$. The filled points were obtained in a separate run, months after the open points, the tube having suffered additional damage. The four solid curves in (a) show a numerical integration of Eq. (36). The four dashed curves represent the low-$n_H$ approximation, calculated using Eqs. (B12) and (B15), with different time scales shown in (a) and (b).

Unfortunately, our apparatus was so prone to developing leaks while it ran that we obtained no data at higher amplitude and never came close to reaching steady-state $n(x)$.

## V. PRACTICAL LESSONS LEARNED

The mathematics developed here makes the concept of peristaltically driving a long, flexible-walled thermoacoustic mixture-separation tube to produce highly enriched isotopes seem promising. This method is inherently less energy efficient[16] than centrifugation, so it is unlikely to be practical for large-scale industrial applications such as uranium enrichment. But the low cost and simplicity of acoustic technology suggest that thermoacoustics might be useful for enrichment of isotopes for research purposes. For example, tenfold to 100-fold pre-enrichment of $^{39}$Ar before atom-trap measurement of the ratio $^{39}$Ar/$^{40}$Ar could enable cost-effective radiometric dating of deep-ocean water, ground water, and ice that have been isolated from contact with the atmosphere for tens to thousands of years.[17] The tiny sample volumes required for this particular application pose special challenges of miniaturization.

The low-amplitude, short-term measurements reported here confirm the related aspects of the mathematics. However, a better tube-fabrication method must be developed to allow long-term, reliable operation.

Equation (A13) shows that the stress in the flexing tube wall during these experiments was about 30 MPa, roughly an order of magnitude smaller than the fatigue strength of stainless steel. Nevertheless, the tube failed repeatedly after only days or weeks of flexure. A significant minority of the failures occurred at places that had no obvious, macroscopic damage. Larger $\epsilon$ or smaller $h/a$ would reduce stress significantly, as shown in Fig. 8.

## ACKNOWLEDGMENTS

This work was supported by the Office of Basic Energy Sciences in the U.S. Department of Energy's Office of Science. We thank Robert Keolian for suggesting that we consider the hydraulic drive mechanism.

## APPENDIX A: RACETRACK RESPONSE TO PRESSURE

Let $a$ and $b$ be the semi-minor and semi-major axes, respectively, of the tube whose cross section is the racetrack-shaped oval shown in Fig. 7, and define

$$\epsilon = b/a - 1. \tag{A1}$$

For a racetrack thin enough that its perimeter stays constant when it changes shape in response to internal pressure $p$, Timoshenko[18] derived the bending moment per unit length, $M$, in the wall,

$$M = pa^2\left(m_0 + y^2/2a^2\right), \text{ straight part,} \tag{A2}$$

$$M = pa^2\left(m_0 + \epsilon\sin\phi + \epsilon^2/2\right), \text{ curved part,} \tag{A3}$$

where

$$m_0 = -\frac{2\epsilon/\pi + \epsilon^2/2 + \epsilon^3/3\pi}{1 + 2\epsilon/\pi}. \tag{A4}$$

The deflection $u$ outward in response to pressure is found by solving

$$\frac{d^2u}{dy^2} = \frac{M}{EI}, \text{ straight part,} \tag{A5}$$

$$\frac{d^2u}{a^2d\phi^2} + \frac{u}{a^2} = \frac{M}{EI}, \text{ curved part,} \tag{A6}$$

where $E$ is the elastic modulus of the tube wall and $I = h^3/12$ with $h$ the thickness of the tube wall, subject to four boundary conditions: The deflection and its tangent must match where the straight and curved parts join, and $du/dy = 0$ at $y = 0$ and $du/d\phi = 0$ at $\phi = \pi/2$ by symmetry. The solution is

$$\frac{u(y)}{a} = \frac{u(y=0)}{a} + \frac{pa^3}{EI}\left(\frac{m_0}{2}\frac{y^2}{a^2} + \frac{1}{24}\frac{y^4}{a^4}\right), \tag{A7}$$

$$\frac{u(\phi)}{a} = \frac{pa^3}{EI}\left[m_0 + c\sin\phi + \frac{\epsilon}{2}\left(\frac{\pi}{2} - \phi\right)\cos\phi + \frac{\epsilon^2}{2}\right], \tag{A8}$$

where

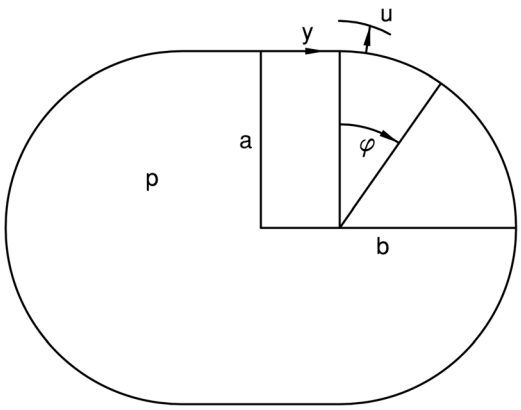


FIG. 7. The top-right quadrant of the thin shell runs clockwise from $y = 0$ to $y = b - a$ along the straight part and then from $\phi = 0$ to $\phi = \pi/2$ along the curved part. Internal pressure $p$ causes deflection $u$, taken to be positive outward.

$$\frac{u(y=0)}{a} = \frac{pa^3}{EI}\left[m_0 + \pi\epsilon/4 + (1 - m_0)\epsilon^2/2 - \epsilon^4/24\right], \tag{A9}$$

$$c = (1 + 2m_0)\,\epsilon/2 + \epsilon^3/6. \tag{A10}$$

Integrating $u$ gives the area change $\delta S/4$ of one quadrant of the racetrack. Normalizing $\delta S$ by the undistorted area $S_m = (1 + 4\epsilon/\pi)\,\pi a^2$ of the racetrack gives the fractional area change in response to pressure,

$$\frac{\delta S}{S_m} = \frac{p}{\beta E}, \tag{A11}$$

where

$$\beta^{-1} = \frac{48a^3/\pi h^3}{1 + 6\epsilon/\pi + 8\epsilon^2/\pi^2} \times \left[\left(\frac{\pi}{4} - \frac{2}{\pi}\right)\epsilon^2 + \frac{\epsilon^3}{2} + \frac{4\epsilon^4}{3\pi} + \frac{2\epsilon^5}{15} + \frac{2\epsilon^6}{45}\right]. \tag{A12}$$

The maximum stress $\sigma_{\max}$ and moment $M_{\max}$ are related by $\sigma_{\max} = 6|M_{\max}|/h^2$. Although the maximum deflection $u_{\max}$ always occurs at $y = 0$, the maximum stress occurs at $y = 0$ for $\epsilon \lesssim 1.09$ and at $\phi = \pi/2$ for $\epsilon \gtrsim 1.09$. Expressing the maximum stress in terms of $\delta S/S_m$ yields

$$\frac{\sigma_{\max}}{E} = 6\max\left[|m_0|, |m_0 + \epsilon + \epsilon^2/2|\right]\left(\beta\frac{a^3}{h^3}\right)\frac{h}{a}\frac{\delta S}{S_m}. \tag{A13}$$

These functions, suitably normalized, are plotted in Fig. 8. For a desired $\delta S/S_m$, the stress can be reduced by reducing the wall thickness $h$ or by increasing $\epsilon$.

## APPENDIX B: LIMITING CASES OF $n_H(x, t)$

In this appendix, we present two analytical solutions to Eq. (36) that we have found for limiting cases. These expressions are useful for checking numerical results. We neglect the dependences of gas properties on $n_H$ and thus on $x$.

### 1. Steady-state solution

In steady state, Eq. (36) becomes

$$0 = Un_H(1 - n_H) + Ddn_H/dx. \tag{B1}$$

With the condition that

$$\int_0^L n_H\,dx = n_{\text{fill}}L, \tag{B2}$$

where $n_{\text{fill}}$ is the mole fraction uniformly filling the tube before enrichment commences, the solution to differential Eq. (B1) can be written compactly as

$$\frac{n_H}{1 - n_H} = \frac{1 - e^{-n_{\text{fill}}\mathcal{P}}}{e^{-n_{\text{fill}}\mathcal{P}} - e^{-\mathcal{P}}}e^{-\mathcal{P}x/L}, \tag{B3}$$

where $\mathcal{P} = UL/D$. The ratio on the left-hand side is called the separation factor in the mixture-separation literature, and it tends to scale exponentially with the size of the system for many isotope-enrichment techniques, as it does here.

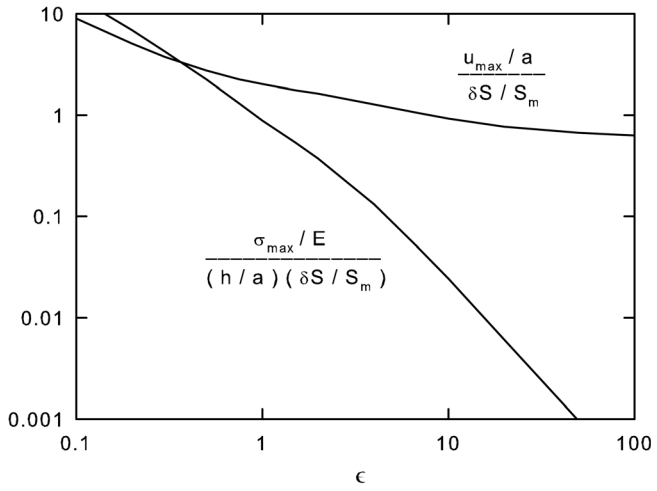


FIG. 8. The maximum displacement and maximum stress of the racetrack-shaped shell as functions of $\varepsilon$.

Figure 9 shows Eq. (B3) for two pressure amplitudes: 0.7 kPa, which is the value we used in the enrichment measurements shown in Fig. 6, and 4.5 kPa, which we hope would be achievable in a more reliable apparatus. In the latter case, $n_{22}$ reaches 0.004 and 0.374 at the ends of the tube, equivalent to a separation factor ratio of two orders of magnitude: In this tube, every 27 turns of the coil would produce a tenfold change in the separation factor at 4.5 kPa. The inset in Fig. 9 shows how $\mathcal{P} = UL/D$ varies with pressure amplitude; the steady-state enrichment falls off rapidly below about 2 kPa, as the $D_{12}$ term in $D$ becomes important.

### 2. Time-dependent solution for small $n_H$

In the limit of low $n_H$, i.e., neglecting the $2n_H$ term in Eq. (36), an analytical solution for $n_H(x,t)$ can be developed by following the outline of Brenner[19] to transform this problem into something that resembles a problem that is treated by Carslaw and Jaeger in *Conduction of Heat in Solids*.[20] Again let $\mathcal{P} = UL/D$. (Our $\mathcal{P}$ is four times larger than Brenner's.) Substituting

$$n_H(x,t) = v(x,t)e^{-\mathcal{P}x/2L - \mathcal{P}Ut/4L} \tag{B4}$$

into Eqs. (36), (39), and (40) in the limit of low $n_H$ yields

$$\frac{\partial v}{\partial t} = D\frac{\partial^2 v}{\partial x^2}, \tag{B5}$$

$$v(x,0) = n_{\text{fill}}e^{\mathcal{P}x/2L} \quad \text{for all } x, \tag{B6}$$

$$v + \frac{2L}{\mathcal{P}}\frac{\partial v}{\partial x} = 0 \quad \text{at } x = 0 \text{ and } x = L, \quad \text{for all } t > 0. \tag{B7}$$

This transformation has eliminated the $\partial/\partial x$ term from the differential equation, putting the problem in the realm of a diffusion equation without convection. Substitution shows that the particular solution

$$v = n_{\text{fill}}\frac{\mathcal{P}}{1 - e^{-\mathcal{P}}}e^{-\mathcal{P}x/2L + \mathcal{P}Ut/4L} \tag{B8}$$

satisfies Eqs. (B5) and (B7). To build up the general solution that also satisfies Eq. (B6), follow Carslaw and Jaeger's Sec. 3.9, trying

$$v \sim e^{-s^2Dt}(G\cos sx + J\sin sx). \tag{B9}$$

Substitution shows that this satisfies Eq. (B5) for any $s$. Applying the $x = 0$ boundary condition shows that

$$J = -\frac{\mathcal{P}}{2sL}G, \tag{B10}$$

and then applying the $x = L$ boundary condition shows that $\sin sL = 0$, so $s_j = j\pi/L$ for $j = 0, 1, 2, \ldots$. Then the general solution should be of the form

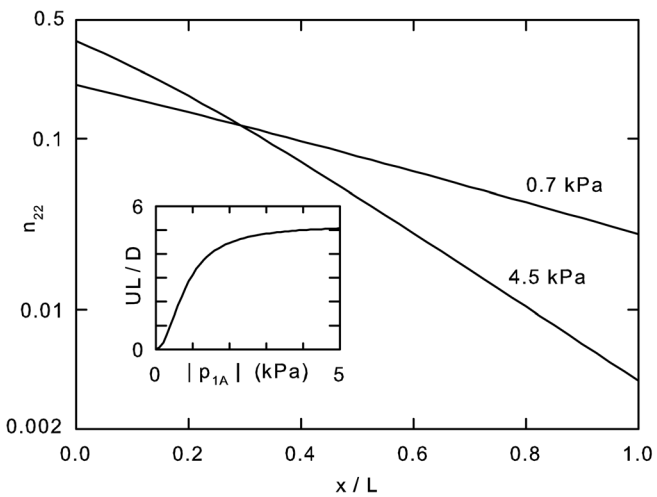


FIG. 9. Predicted $x$ dependence of steady-state mole fraction $n_{22}$ in our apparatus at the mid-tube pressure amplitude used for enrichment measurements shown in Fig. 6 (0.7 kPa) and at a higher amplitude that should be accessible with better tubing and drivers (4.5 kPa; $|p_{1A}|/p_m = 0.05$). The average of each curve is $n_{\text{fill}} = 0.092$. Inset: The dependence of $UL/D$ on pressure amplitude in our apparatus.

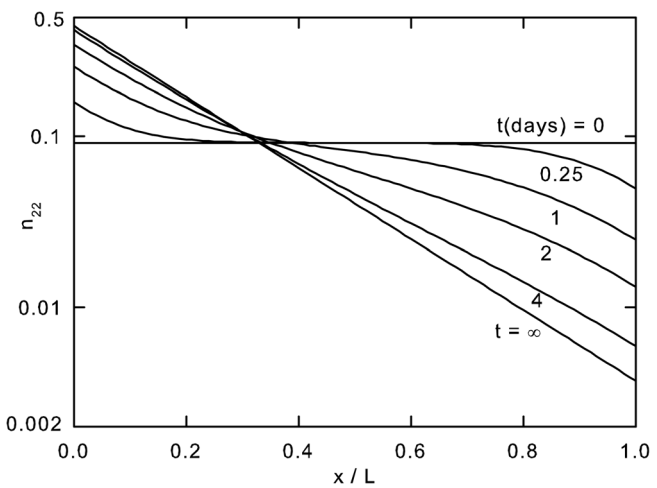


FIG. 10. The result of Eqs. (B12) and (B15) for our apparatus with $|p_{1A}| = 4.5$ kPa. At the high-$n_{22}$ end, the $t = \infty$ curve differs slightly from the 4.5-kPa curve in Fig. 9 because of the neglect of the $2n_H$ term in Eq. (36) here.

$$v(x,t) = n_{\text{fill}} \frac{\mathcal{P}}{1-e^{-\mathcal{P}}}\, e^{-\mathcal{P}x/2L+\mathcal{P}Ut/4L} + \sum_{j=1}^{\infty} e^{-j^2\pi^2 Dt/L^2} G_j \left(\cos\frac{j\pi x}{L} - \frac{\mathcal{P}}{2j\pi}\sin\frac{j\pi x}{L}\right), \tag{B11}$$

$$n_H(x,t) = n_{\text{fill}} \frac{\mathcal{P}}{1-e^{-\mathcal{P}}}\, e^{-\mathcal{P}x/L} + e^{-\mathcal{P}x/2L-\mathcal{P}Ut/4L} \sum_{j=1}^{\infty} e^{-j^2\pi^2 Dt/L^2} G_j \times \left(\cos\frac{j\pi x}{L} - \frac{\mathcal{P}}{2j\pi}\sin\frac{j\pi x}{L}\right). \tag{B12}$$

(Note how the $j = 0$ term turns out to be zero.)

Integrating products of the functions

$$\psi_m = \cos mx - \frac{Q}{2m\pi}\sin mx, \quad m = 1, 2, \ldots, \tag{B13}$$

from 0 to $\pi$ shows that they are an orthogonal set on that interval. They are also a complete set because they satisfy Theorem 1 in Ref. 21 for $\phi_m = \cos mx$, $q = 0$, $\lambda = m^2$, and $\alpha_1/\alpha = \beta_1/\beta = 2\pi/Q$. Then the $G_j$ can be obtained from the initial condition, Eq. (B6), expressed in terms of Eq. (B11), via an integral similar to taking a finite Fourier transform,

$$G_{1j} = \frac{2}{\pi}\left(1+\frac{\mathcal{P}^2}{4j^2\pi^2}\right)^{-1} n_{\text{fill}} \int_0^{\pi} \left(e^{\mathcal{P}y/2\pi} - \frac{\mathcal{P}}{1-e^{-\mathcal{P}}} e^{-\mathcal{P}y/2\pi}\right) \times \left(\cos jy - \frac{\mathcal{P}}{2j\pi}\sin jy\right) dy, \tag{B14}$$

$$= \frac{2\mathcal{P}}{j^2\pi^2}\left(1+\frac{\mathcal{P}^2}{4j^2\pi^2}\right)^{-2} n_{\text{fill}} \left[(-1)^j e^{\mathcal{P}/2} - 1\right]. \tag{B15}$$

Equations (B12) and (B15) comprise a general solution to Eqs. (36), (39), and (40) when the $2n_H$ term in Eq. (36) can be neglected (Fig. 10).


[1]G. W. Swift and P. S. Spoor, "Thermal diffusion and mixture separation in the acoustic boundary layer," J. Acoust. Soc. Am. **106**, 1794–1800 (1999); **107**, 2299(E) (2000); **109**, 1261(E) (2001).
[2]D. A. Geller and G. W. Swift, "Saturation of thermoacoustic mixture separation," J. Acoust. Soc. Am. **111**, 1675–1684 (2002).
[3]G. W. Swift and D. A. Geller, "Continuous thermoacoustic mixture separation," J. Acoust. Soc. Am. **120**, 2648–2657 (2006); **124**, 2421(E) (2008).
[4]D. A. Geller and G. W. Swift, "Thermoacoustic enrichment of the isotopes of neon," J. Acoust. Soc. Am. **115**, 2059–2070 (2004).
[5]R. C. Jones and W. H. Furry, "The separation of isotopes by thermal diffusion," Rev. Mod. Phys. **18**, 151–224 (1946).
[6]C. C. Lawrenson, L. D. Lafleur, and F. D. Shields, "The solution for the propagation of sound in a toroidal waveguide with driven walls (the acoustitron)," J. Acoust. Soc. Am. **103**, 1253–1260 (1998).
[7]Tube Methods, Inc., Bridgeport, PA.
[8]Endevco, San Juan Capistrano, CA, www.endevco.com (Last viewed October 2013). Model 8510B-50 in the neon, 8510B-500 in the water. Although using these transducers in water is not recommended by the manufacturer, we found that the 8510B-500 will endure wet operation for months at a time.
[9]RGA100, Stanford Research Systems, Sunnyvale CA, www.thinksrs.com (Last viewed October 2013).
[10]Model FC-16, 1-in o.d., 10 convolutions, Servometer, Cedar Grove NJ, www.servometer.com (Last viewed October 2013).
[11]Model GW-205/8S Pismo poly woofer, Goldwood Sound, Inc., Chatsworth CA, www.goldwoodsound.com (Last viewed October 2013).
[12]G. W. Swift, *Thermoacoustics: A Unifying Perspective for Some Engines and Refrigerators* (Acoustical Society of America Publications, Sewickley, PA, 2002).
[13]To arrive at Eq. (9), integrate the first-order continuity equation $\partial\rho_1/\partial t + \rho_m \nabla \cdot \mathbf{v}_1 = 0$ over the cross-sectional area of the channel and apply the divergence theorem to the integral of the $y, z$ terms in the divergence.
[14]The phase measurements seemed erratic at the lowest amplitudes, so the phase measurements of points with $|p_1|/|P_1| < 0.01$ in Figs. 3 and 4 may be erroneous.
[15]Wolfram MATHEMATICA 9, NDSolveValue, with AccuracyGoal = PrecisionGoal = 12, and with boundary conditions (40) suppressed near $t = 0$ with a 3-min exponential time constant to soften the $t = 0$ numerical conflict with boundary condition (39).
[16]D. A. Geller and G. W. Swift, "Thermodynamic efficiency of thermoacoustic mixture separation," J. Acoust. Soc. Am. **112**, 504–510 (2002).
[17]Z.-T. Lu, "What trapped atoms reveal about global groundwater," Phys. Today **66**, 74–75 (2013).
[18]S. Timoshenko, *Strength of Materials, Part I: Elementary Theory and Problems*, 3rd ed. (Van Nostrand, Princeton, 1955), p. 388.
[19]H. Brenner, "The diffusion model of longitudinal mixing in beds of finite length," Chem. Eng. Sci. **17**, 229–243 (1962).
[20]H. S. Carslaw and J. C. Jaeger, *Conduction of Heat in Solids*, 2nd ed. (Oxford University Press, Oxford, UK, 1959).
[21]G. Birkhoff and G.-C. Rota, "On the completeness of Sturm–Liouville expansions," Am. Math. Monthly **67**, 835–841 (1960).